Energy Dissipation Analysis for Elastoplastic Contact and Dynamic Dashpot Models

Gengxiang Wang (wanggengxiang@pku.edu.cn)
Caishan Liu† (liucs@pku.edu.cn)
State Key Laboratory for Turbulence and Complex Systems, College of Engineering, Peking University, Beijing, 100871, China
Yang Liu (y.liu2@exeter.ac.uk)
College of Engineering, Mathematics and Physical Sciences, University of Exeter, North Park Road, Exeter, EX4 4QF, UK

ABSTRACT

This investigation aims to analyze the underlying relationship between the dynamic dashpot and the static force-displacement models used in multibody systems. By ignoring the plastic flow of the contact body made of elastoplastic material, the coefficient of restitution of the dynamic dashpot model can be calculated by using the static force-displacement model proposed by Ma and Liu (Ma-Liu model). Simulation results show the consistency of energy dissipation between the Ma-Liu model and Flores et al. model, but there are still slight differences. This is because the Hertz contact stiffness of the dynamic dashpot model overestimates the actual contact stiffness in the elastoplastic phase. Therefore, in order to eliminate this discrepancy when depicting energy dissipation during impact, the Hertz contact stiffness can be replaced by the linearized elastoplastic contact one from the Ma-Liu model; subsequently, a new hysteresis damping factor is derived based on the linearized elastoplastic contact stiffness and energy conservation during impact. Finally, a new elastoplastic dashpot model can be obtained by the elastoplastic contact stiffness combined with a new hysteresis damping factor. To verify the practicability and effectiveness of the new model, a granular chain and a slider-crank mechanism with a clearance joint are employed as numerical examples.

Keywords: Energy dissipation; Static elastoplastic model; Elastoplastic dashpot model; Coefficient of Restitution; Multibody system

Nomenclature:

A — the amplitude

c_r — Newton's coefficient of restitution

E_1 and E_2 — Young's modulus

ΔE — the dissipated energy

ΔE_c — the dissipated energy in the compression phase

ΔE_r — the dissipated energy in the recovery phase

F — the loading force or contact force

F_s — from the Ma-Liu model

F_d — from the dynamic dashpot model

K_p — the linearized contact stiffness in the elastoplastic or plastic phase

K_e — the Hertz contact stiffness

m — the mass of the contact body

m_1 and m_2 — the mass of two contact bodies

n — the power exponent

p_y — the critical value of yielding

R_1 and R_2 — the radii of curvature of the contact bodies

R_{ep}^e — the radius of curvature after impact in the elastoplastic phase

R_p^e — the radius of curvature after impact in the plastic phase

U — the work done by the contact force at the end of the loading phase

$U^{(\max)}$ — the maximum stored strain energy

ΔU — the energy dissipation from the static Ma-Liu model

v_0 — the initial impact velocity

v_1 and v_2 — the initial impact velocities of two contact bodies

W — the work done by the contact force during the unloading phase

ν_1 and ν_2 — the Poisson ratio

σ_y — the yield stress

δ — the contact deformation

δ_y — the critical elastic deformation

δ_{ep} — the elastoplastic deformation

δ_p — the critical plastic deformation

δ_r — the residual deformation

$\delta_{\max}$ — the maximum deformation

$\dot{\delta}^{(-)}$ — the initial compressive velocity

$\dot{\delta}^{(+)}$ — the relative separating velocity

$\dot{\delta}$ — the relative impact velocity

ξ and ψ — the dimensionless parameters

χ — the hysteresis damping factor

1. Introduction

Collision events widely exist in nature and various engineering problems [1][2]. The main issue lies in how to quantify energy dissipation during contact. It is observed that the energy dissipation [3] caused by a collision is usually closely related to the impact velocity $\dot{\delta}_i$, which is intuitively believed to be related to the viscous effect of the materials. Therefore, a dashpot model, that consists of a linear or nonlinear parallel spring-dashpot assembly [4], is often adopted to describe the interaction between two colliding bodies. These dashpot models [5] usually consist of a damping factor (χ) [6,7] expressed as a function of coefficient of restitution (CoR) [8–10], impact velocity and contact stiffness K, i.e., $\chi=\chi\left(c_r,\dot{\delta}_i,K\right)$, where c_r stands for CoR. Raising questions related to the dashpot models are as follows: (i) How to obtain the function $\chi=\chi\left(c_r,\dot{\delta}_i,K\right)$; (ii) How to determine the value of CoR [11]. To answer these questions, an overview of historical development on this topic is needed.

Kelvin and Voigt (KV) [12] were pioneers using damping factors to measure the energy dissipation

during impact [12–15]. In this model, the contact force was described as a parallel linear spring-damper element as $F=K_0\delta+D_0\dot{\delta}$, where K_0 is a constant contact stiffness, D_0 is a constant damping coefficient, δ and $\dot{\delta}$ are the relative contact deformation and contact velocity, respectively. It is obvious that the model provides nonzero contact force at the beginning and end of the impact [12], which is not suitable for cohesionless materials. Hunt and Crossley (HC) [16] described the contact force by using the Hertz contact law with a nonlinear viscous-elastic element, i.e., $F=K_e\delta^n+D\dot{\delta}$, where K_e is the Hertz contact stiffness [17]. The damping coefficient in the HC model is set as $D=\chi\delta^n$, where χ is the hysteresis damping factor that is related to the value of CoR [18]. Since the HC model can avoid the discontinuity of the contact force at the initial instant and the end of the contact, this model promoted several studies on how to evaluate the damping coefficient, and in turn resulting in several variations on the original HC model [19]. The most feasible model was given by Lankarani and Nikravesh [20,21], in which the CoR [11,22,23] was assumed to be an independent constant. However, Zhang and Sharf [24] experimentally demonstrated that the HC model could only perform well in a near elastic impact scenario. When plastic deformation during contact becomes more significant [16,25], the prediction accuracy of the model is very low.

For analyzing the collision process, the consistency of system energy should be maintained no matter which model is used. Lankarani et al. [20][21] and Ye et al. [26] pointed out that although the HC model can successfully avoid force inconsistency caused by the KV model, it cannot achieve energy consistency. In other words, the HC model, even when used to deal with a normal collision between a ball and a wall, cannot produce an output CoR that equals to the input CoR used to compute the hysteresis damping factor. Flores et al. model [27] constructed a single degree of freedom spring-damping system, from which a relationship between deformation δ and deformation velocity $\dot{\delta}$ was established. This relationship was then used to compute the work done by the damping force component. Based on the balances of energy and linear momentum during an impact motion [27,28], a relationship between the hysteresis damping factor χ and the CoR can be established [29]. This model can keep the consistency of the system energy well, but its CoR was considered as a material constant [30], and the Hertz contact stiffness was used in the linear spring-damper element [31]. In our previous numerical studies and experiments [32], it was shown that the CoR was not a material constant [9,10,33,34], and its value can change with impact velocity. This was due to an increase in energy absorption at higher impact velocities during plastic deformation [35–37]. In addition, Hertz contact stiffness is only applicable for the elastic contact. When plasticity occurs [38], the contact stiffness varies greatly, see e.g., [32,39,40].

Another way of modeling contact is from the force-displacement relationship [23,41], which is usually established by analyzing the static contact process. Greenwood and Williamson [42] developed a static plastic contact model for two rough surfaces. Zhao et al. [43] presented an elastic-plastic asperity microcontact model applied between two nominally flat surfaces. By using the finite element method, Kogut and Etsion [13] provided simple analytical models for the elastic, elastoplastic and plastic contact deformation phases. Stronge [36] employed an approximate approach to study the mixed elastic-plastic and full plastic regimes. Thornton [25] proposed a simplified theoretical model

for the normal contact interaction between two elastic-full plastic spheres based on the discrete element code. Du and Wang [44] proposed a theoretical model of elastoplastic impact for two spheres, including the elastic, elastoplastic and full plastic phases, and used the finite element method to verify its correctness. Brake [45] presented a mixed elastic-plastic regime by enforcing continuity between the elastic and fully plastic regimes. Burgoyne and Daraio [46] provided an elastoplastic contact model for describing the collision between particles in the granular chain. Our recent work [31] developed an elastic-plastic contact model, namely the Ma-Liu model, which can describe the force-displacement relationship of the contact in elastic, elastoplastic and plastic contact phases. It was validated using the experimental data found in [47] in terms of the force-displacement curves and the CoR, and the proposed four-phase model was in good agreement with these experiments.

This paper aims to establish the relationship between the dashpot model and the force-displacement model for rate-independent (elastic or plastic behavior) materials [37]. According to the material properties of the contact body, including Young's modulus and yield strength, the force-displacement relationship was determined by the Ma-Liu model [32], and the contact stiffness was then obtained from the force-displacement curve. Thus, the CoR was equal to the square root of ratio of the area below the curve during unloading (restitution) to that of during loading (compression) [16,48,49]. The computed contact stiffness and CoR were taken as the input parameters for the dashpot models [50–52]. The second objective of the present work is to compare energy dissipation [53], the maximum contact force [54], and post-impact velocity [1] obtained by both models under the same energy inputs. If they are very close to each other, we can conclude that these two models, i.e., the static elastoplastic contact model [45] and the dynamic dashpot model [3][55], are approximately equivalent. Therefore, the data observed by a simple compression experiment could be applied to model the impact process, and vice versa [56]. In this work, we check the equivalence by choosing three different dashpot models, including the HC model, the Lankarani-Nikravesh (LN) model and the Flores et al. model. We will show that the first two dashpot models cannot achieve energy consistency, but the Flores et al. one can although some slight differences exist. This is due to the Hertz contact stiffness in the Flores et al. model that overestimates the actual contact stiffness in the elastoplastic or the plastic contact phase. Therefore, we follow the methodology adopted in the Flores et al. model to propose a new dashpot model [26][27], which replaces the Hertz contact stiffness by using a linear elastoplastic contact stiffness for deriving the explicit relationship between the CoR and a hysteresis damping factor. Finally, two examples, a granular chain subject to collisions [57][58,59] and a slider-crank mechanism with a clearance joint [60], are studied to test the efficacy of the proposed dashpot model.

The rest of the paper is organized as follows. In Section 2, the Ma-Liu model is introduced briefly, and the new dashpot model is proposed in Section 3. The equivalent relationship between the static elastoplastic contact model and the dynamic dashpot model is discussed in Section 4. In Section 5, a horizontal granular chain and a slider-crank mechanism with a clearance joint are studied. Finally, conclusions are drawn in Section 6.

2. Static elastoplastic contact model

Fig.1 illustrates four phases of a contact behavior between two spheres, including elastic,

elastoplastic, and plastic deformations. The masses of these two contact bodies are m_1 and m_2 with their initial impact velocities are v_1 and v_2, respectively. As can be seen from the figure, it shows the critical elastic deformation δ_y at the compression phase, the deformation δ_{ep} at the elastoplastic compression phase, the critical plastic deformation δ_p at the compression phase, and the residual deformation δ_r at the restitution phase. There are critical elastic and plastic deformation boundaries that switch the contact condition of these two colliding spheres within these phases.

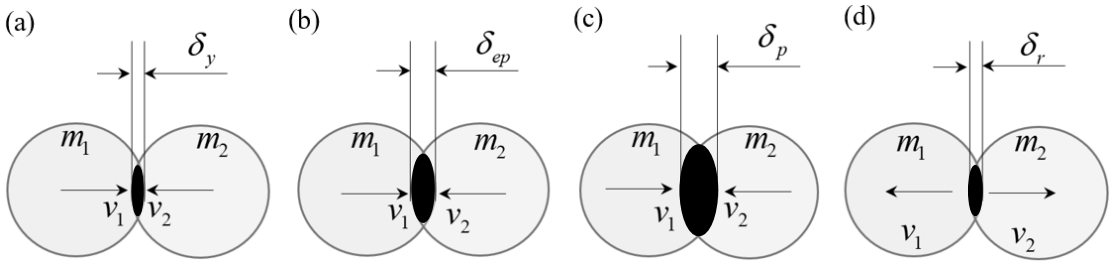

Fig.1 Contact procedure between two colliding spheres: (a) elastic compression phase, (b) elastoplastic compression phase, (c) plastic compression phase, and (d) recovery phase.

2.1. Ma-Liu static contact force model

Compared to the existing dynamic dashpot models [13,14], the static elastoplastic contact models in [40,45] have different constitutive relations between the loading and unloading paths. To understand the constitutive relation from the Ma-Liu model [32], which can accurately describe the contact stiffness in the elastoplastic or plastic phase, it is necessary to introduce this elastoplastic contact model in detail in this subsection.

According to Ma and Liu [32], the loading phase of the Ma-Liu model is governed by

$$F(\delta)=\begin{cases}\dfrac{4}{3}ER^{\frac{1}{2}}\delta^{\frac{3}{2}} & \delta<\delta_y\\ \delta\left(c_1+c_2\ln\dfrac{\delta}{\delta_y}\right)+c_3 & \delta_y\le\delta<\delta_p\\ F_p+k_1\left(\delta-\delta_p\right) & \delta\ge\delta_p\end{cases} \tag{1}$$

where the effective elastic modulus and radius are expressed as $1/E=\left(1-\nu_1^2\right)/E_1+\left(1-\nu_2^2\right)/E_2$, $R=R_1R_2/\left(R_1\pm R_2\right)$, R_1 and R_2 are the radii of curvatures of the contact bodies, E_1 and E_2 are Young's moduli of the contact bodies, ν_1 and ν_2 are the Poisson ratios of the contact material, $\delta_y=\pi^2Rp_y^2/4E^2$ is the critical elastic deformation, $p_y=1.61\sigma_y$ is the critical value of yielding, σ_y is the yield stress, and $\delta_p=\xi^2\delta_y/2$ is the critical plastic deformation. ξ is a dimensionless parameter indicating when the pressure on the contact surface approximately approaches to uniformity. Its value

is within the scope from 13 to 20 when the contact spheres are made of the same materials [32]. The specified forms of the coefficients in this contact model can be expressed as

$$\begin{cases} k_1 = 2\pi R\psi\sigma_y, \quad F_p = \delta_p\left(c_1 + c_2\ln\left(\xi^2/2\right)\right) + c_3 \\ c_1 = \dfrac{p_y\left(1+\ln\left(\xi^2/2\right)\right) - 2\psi\sigma_y}{\ln\left(\xi^2/2\right)}\pi R, \quad c_2 = \dfrac{2\psi\sigma_y - p_y}{\ln\left(\xi^2/2\right)}\pi R \\ c_3 = F_y - c_1\delta_y, \quad F_y = \pi^3 R^2 p_y^3/6E^2 \end{cases} \tag{2}$$

where ψ is a dimensionless parameter that corresponds to the ratio between the Brinell hardness and the yielding strength of the material ranging from 2.6 to 3.0 [32].

During the unloading phase, the constitutive relation between the contact force and the displacement is given as

$$F(\delta) = \begin{cases} \dfrac{4}{3}ER^{\frac{1}{2}}\delta^{\frac{3}{2}} & \delta_{\max} < \delta_y \\ \dfrac{4}{3}E\left(R^e\right)^{\frac{1}{2}}\left(\delta - \delta_r\right)^{\frac{3}{2}} & \delta_y \le \delta_{\max} < \delta_p \\ \dfrac{4}{3}E\left(R_p^e\right)^{\frac{1}{2}}\left(\delta - \delta_r\right)^{\frac{3}{2}} & \delta_{\max} \ge \delta_p \end{cases} \tag{3}$$

Since both elastoplastic and plastic deformations occur before the restitution phase, the curvature radius of the contact bodies is larger than the one before plastic deformation. Therefore, when the contact behavior terminates at the elastoplastic compression phase, the radius of curvature of the contact body can be written as

$$R_{ep}^e = \frac{F^e R}{F_{\max}}, F^e = \frac{4}{3}ER^{\frac{1}{2}}\delta_y^{\frac{3}{2}} \tag{4}$$

where R_{ep}^e is the radius of curvature after the impact in the elastoplastic phase.

When the contact behavior ends at the plastic compression phase, the radius of curvature of the contact body can be written as

$$R_p^e = \frac{F_p^e R}{F_{ep}}, F_p^e = \frac{4}{3}ER^{\frac{1}{2}}\delta_p^{\frac{3}{2}} \tag{5}$$

where R_p^e is the radius of curvature after the impact in the plastic phase. F_{ep} and δ_p are the load and critical plastic contact deformation at the beginning of the plastic contact phase, respectively.

To illustrate the force-deformation relationship of the Ma-Liu model, a sketch diagram is presented in Fig.2. It can be clearly seen that such a relationship is very similar to the linear relation in the elastoplastic or the plastic phase, while the nonlinear elastic contact phase occurs within a short period at the beginning of the entire contact behavior.

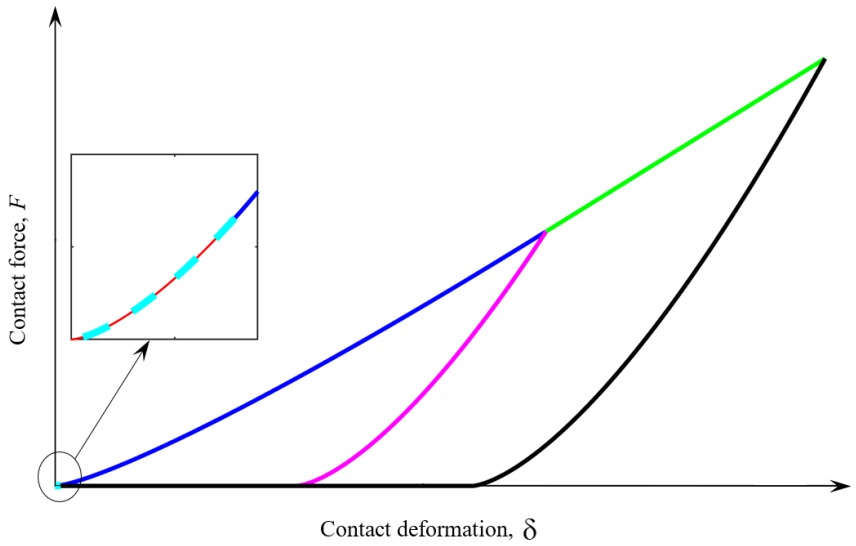

Fig.2 Sketch diagram of the relationship between the contact force and the contact deformation based on the Ma-Liu model, where red line is the elastic deformation in the compression phase, blue line is the elastoplastic deformation in the compression phase, green line is the plastic deformation in the compression phase, cyan dashed line is the elastic deformation in the recovery phase, purple line is the elastoplastic deformation in the recovery phase, and black line is the plastic deformation in the recovery phase.

2.2. Coefficient of restitution

Since the energy dissipation during an impact is inevitable [35,61,62], the CoR severs as a crucial parameter used to represent the energy dissipation caused by the seismic waves [63] and the elastoplastic deformation during the contact of dissimilar bodies [11]. In general, there are three different formulations of CoR: (i) Newton' s CoR [9,16] is the ratio between the initial and the post-impact velocities; (ii) Poisson's CoR [10] is the ratio of the impulse between the compression and the recovery phases; (iii) Stronge's CoR [36] is the ratio of the work done by the contact forces between the compression and the recovery phases. Although the CoR has different definitions, they should be equivalent regarding to the same impact scenario. In Section 4, this conclusion will be validated by the Newton's and the Stronge's CoRs. In the following sections, we will employ the Stronge's CoR used in the Ma-Liu model [32].

The energy U is equal to the work done by the contact force at the end of the loading phase, which can be written as

$$U=\frac{1}{2}mv_0^2=\begin{cases}\dfrac{8}{15}ER^{\frac{1}{2}}\delta_{\max}^{\frac{5}{2}} & \delta_{\max}<\delta_y \\ \dfrac{8}{15}ER^{\frac{1}{2}}\delta_y^{\frac{5}{2}}+\left(\dfrac{1}{2}c_1-\dfrac{1}{4}c_2\right)\left(\delta_{\max}^2-\delta_y{}^2\right)+\dfrac{1}{2}c_2\delta_{\max}^2\ln\dfrac{\delta_{\max}}{\delta_y} & \delta_y\le\delta_{\max}<\delta_p \\ +c_3\left(\delta_{\max}-\delta_y\right) & \\ \dfrac{8}{15}ER^{\frac{1}{2}}\delta_y^{\frac{5}{2}}+\left(\dfrac{1}{2}c_1-\dfrac{1}{4}c_2\right)\left(\delta_p^2-\delta_y{}^2\right)+\dfrac{1}{2}c_2\delta_p^2\ln\dfrac{\delta_p}{\delta_y} & \delta_{\max}\ge\delta_p \\ +c_3\left(\delta_p-\delta_y\right)+F_p\left(\delta_{\max}-\delta_p\right)+\dfrac{1}{2}k_1\left(\delta_{\max}-\delta_p\right)^2 & \end{cases} \tag{6}$$

where v_0 is the initial impact velocity, and the mass is written as $m=m_1m_2/\left(m_1+m_2\right)$.

The work done by the contact force during the unloading phase is written as

$$W=\begin{cases} W^{e}=\dfrac{8}{15}ER^{\frac{1}{2}}\delta_{\max}^{\frac{5}{2}} & \delta_{\max}<\delta_{y} \\ W^{ep}=\dfrac{8}{15}E\left(R^{e}\right)^{\frac{1}{2}}\left(\delta_{\max}-\delta_{r}\right)^{\frac{5}{2}} & \delta_{y}\le\delta_{\max}<\delta_{p} \\ W^{p}=\dfrac{8}{15}E\left(R_{p}^{e}\right)^{\frac{1}{2}}\left(\delta_{\max}-\delta_{r}\right)^{\frac{5}{2}} & \delta_{\max}\ge\delta_{p} \end{cases} \tag{7}$$

Therefore, the definition of the energetic coefficient by Stronge [36] can be expressed as

$$\mathrm{CoR}=\sqrt{\frac{W}{U}}=\begin{cases} 1 & \delta_{\max}<\delta_{y} \\ \sqrt{2W^{ep}/mv_{0}^{2}} & \delta_{y}\le\delta_{\max}<\delta_{p} \\ \sqrt{2W^{p}/mv_{0}^{2}} & \delta_{\max}\ge\delta_{p} \end{cases} \tag{8}$$

3. New dashpot model with a hysteresis damping factor

Since the Hertz contact stiffness overestimates the contact stiffness in the elastoplastic or the plastic phase, it may lead to inaccurate calculations of the energy dissipation, the post-impact velocity, and the maximum contact force during the impact. In order to eliminate or reduce the error caused by the Hertz contact stiffness, the Hertz contact stiffness in the elastoplastic or plastic phase can be represented by the linearized elastoplastic contact stiffness from the Ma-Liu model. If the damping factor is $C=\chi\delta^{n}$, where χ is the new hysteresis damping factor, the power exponent n should equal to 1 rather than 1.5 because of the linear relationship between the contact force and the deformation. Thus, the new dynamic dashpot model can be expressed as

$$F=K_{p}\delta+\chi\delta\dot{\delta},\quad K_{p}=\frac{F\left(\delta_{p}\right)-F\left(\delta_{y}\right)}{\delta_{p}-\delta_{y}} \tag{9}$$

where K_p is the linearized elastoplastic contact stiffness from the Ma-Liu model.

At the end of the compression phase, the maximum stored strain energy corresponding to the maximum deformation can be expressed as [27]

$$U^{(\max)}=\int_{0}^{\delta_{\max}}K_{p}\delta d\delta=\frac{1}{2}K_{p}\delta_{\max}^{2} \tag{10}$$

The dissipated energy through the work done by the damping force can be written as [20]

$$\Delta E=\iint\chi\delta\dot{\delta}d\delta \tag{11}$$

The whole contact process contains two phases: compression and recovery. The entire dissipated energy caused by the damping factor is given as [27]

$$\Delta E=\Delta E_{c}+\Delta E_{r}=\chi\left(\dot{\delta}^{(-)}+\left|\dot{\delta}^{(+)}\right|\right)\int_{0}^{\delta_{\max}}\delta\sqrt{1-\left(\frac{\delta}{\delta_{\max}}\right)^{2}}d\delta \tag{12}$$

where ΔE_c and ΔE_r are the dissipated energy in the compression and recovery phases, respectively. $\dot{\delta}^{(-)}$ and $\dot{\delta}^{(+)}$ are the initial compressive velocity and the relative separating velocity, respectively.

The integral process can be transformed as

$$\Delta E = \Delta E_c + \Delta E_r = \chi\left(\dot{\delta}^{(-)} + \left|\dot{\delta}^{(+)}\right|\right)\delta_{\max}^2 \int_0^1 x\sqrt{1-x^2}\,dx = \frac{1}{3}\chi\left(1+c_r\right)\dot{\delta}^{(-)}\delta_{\max}^2 \tag{13}$$

where $c_r = \dfrac{\left|\dot{\delta}^{(+)}\right|}{\dot{\delta}^{(-)}}$ is the Newton's CoR.

According to the energy balance before and after the collision, the dissipated energy in an entire collision process can be written as

$$\Delta E = \frac{1}{2}m\left(1-c_r^2\right)\left(\dot{\delta}^{(-)}\right)^2 \tag{14}$$

The energy balance at the end of the compression phase can be expressed as

$$\frac{1}{2}m_1 v_1^2 + \frac{1}{2}m_2 v_2^2 = \frac{1}{2}\left(m_1+m_2\right)v_{12}^2 + \frac{1}{2}K_p\delta_{\max}^2 + \frac{1}{3}\chi\dot{\delta}^{(-)}\delta_{\max}^2 \tag{15}$$

Further simplifying Eq. (15) based on the linear momentum balance gives

$$\delta_{\max}^2 = \frac{3m\left(\dot{\delta}^{(-)}\right)^2}{3K_p + 2\chi\dot{\delta}^{(-)}} \tag{16}$$

Combining Eq. (14), Eq. (16) and Eq. (13), the new hysteresis damping factor can be obtained as

$$\chi = \frac{3K_p\left(1-c_r\right)}{2c_r\dot{\delta}^{(-)}} \tag{17}$$

Finally, according to Eq. (9), the new dynamic dashpot model can be formulated as

$$F = K_p\delta\left[1 + \frac{3\left(1-c_r\right)}{2c_r}\frac{\dot{\delta}}{\dot{\delta}^{(-)}}\right] \tag{18}$$

It is worth noting that Eq. (18) is significantly different from the Ma-Liu model. As for the contact material, without considering the strain rate variation, the Ma-Liu model was obtained by a static pressure experiment, which can accurately capture the mechanics features during impact. However, the Ma-Liu model adopts different constitutive relations during contact, including the loading and the unloading paths. This calculation strategy leads to the maximum contact deformation and the residual deformation being saved in each impact for the following contact behavior, which is inefficient in calculating multi-compression and multi-collision events. Therefore, in multibody impact dynamics, the static elastoplastic model (e.g., the Ma-Liu model) was not widely used to calculate the impact process in commercial software, such as EDEM and ADAMS. On the contrary, since the dashpot model utilizes the direction of the impact velocity to distinguish the compression and the recovery phases and forms the hysteresis loop during impact, the entire contact process is governed by Eq. (18) rather than Eq. (1) and Eq. (3). In this case, the residual deformation in each contact is not needed, and identification of the loading and the unloading processes is not required anymore. Thus, the dashpot model remarkably simplifies the calculation process compared to the static elastoplastic model. However, the existing dashpot models [64] employed the Hertz contact stiffness coefficient that overestimated the elastoplastic contact stiffness leading to significant calculation errors. For this reason,

we propose this new elastoplastic dashpot model in the present paper by using a linearized elastoplastic contact stiffness adopted from the Ma-Liu model. This new dashpot model can not only avoid the deficits caused by the Hertz contact stiffness, but also simplify the calculations in multi-compression and multi-collision events in a multibody system.

4. Comparison between the Ma-Liu and the dynamic dashpot models

For the Ma-Liu model, the energy dissipation is depicted by the enclosed area between the loading in Eq. (6) and the unloading path in Eq. (7). For the dashpot models, the dissipated energy from the HC model [16], the LN model [20,21] and the Flores et al. model [27] are expressed as the integration of the damping factor to the contact deformation $\Delta E = \int \chi \delta \dot{\delta} d\delta$. In principle, the area of the enclosed area from the Ma-Liu model should be approximately the same as the area of the hysteresis loop from the dynamic dashpot model, since both closed areas represent the dissipated energies during contact. To reveal the discrepancy between them, the relative error percentages of the energy dissipations and the maximum contact forces for these two models are defined as

$$E_{percentage} = \frac{|\Delta U - \Delta E|}{\Delta U} \times 100\%, \; F_{percentage} = \frac{|F_s - F_d|}{F_s} \times 100\% \tag{19}$$

where ΔE is the energy dissipation from the dynamic dashpot model, ΔU is the energy dissipation from the Ma-Liu model, F_s can be obtained by using the Ma-Liu model, and F_d can be calculated based on the dynamic dashpot model.

Since the CoR can be calculated from the static contact model, it can be determined in advance for the dynamic dashpot model. Based on Eq. (8), the CoR in the Ma-Liu model defined by Stronge is closely related to the dimensionless parameters ξ and ψ. The contact parameters used for comparison are given in Table 1. Considering that the effect of the dimensionless parameters on the CoR in the elastoplastic phase is the same as in the plastic phase, only the relationship between the CoR and the dimensionless parameters in the elastoplastic phase is presented in Fig.3. As can be seen from the figure, the CoR is inversely proportional to the dimensionless parameter ξ, and is proportional to the dimensionless parameter ψ. Considering the existing dynamic dashpot models, which were extended from the Hertz contact law in the elastic phase, most of the kinetic energies are stored in the contact bodies as strain energies, and the dissipated energy represented by the damping factor is negligible. Thus, higher CoRs should be selected for the existing dynamic dashpot models to depict the contact behavior. To reduce the effect of the dimensionless parameters on the CoR, both parameters are chosen as $\psi = 3.0$ and $\xi = 13$.

Table 1. Contact parameters of the impact scenario

Body	Young's modulus	Poisson ratio	Radius	Yield strength	Mass (kg)	Density
Body 1	2.0E11 Pa	0.29	2.05E-2 m	1.03E9 Pa	0.097 kg	7800 kg/m^3
Body 2	6.5E10 Pa	0.33	2.00E-2 m	3.00E7 Pa	0.261 kg	2700 kg/m^3

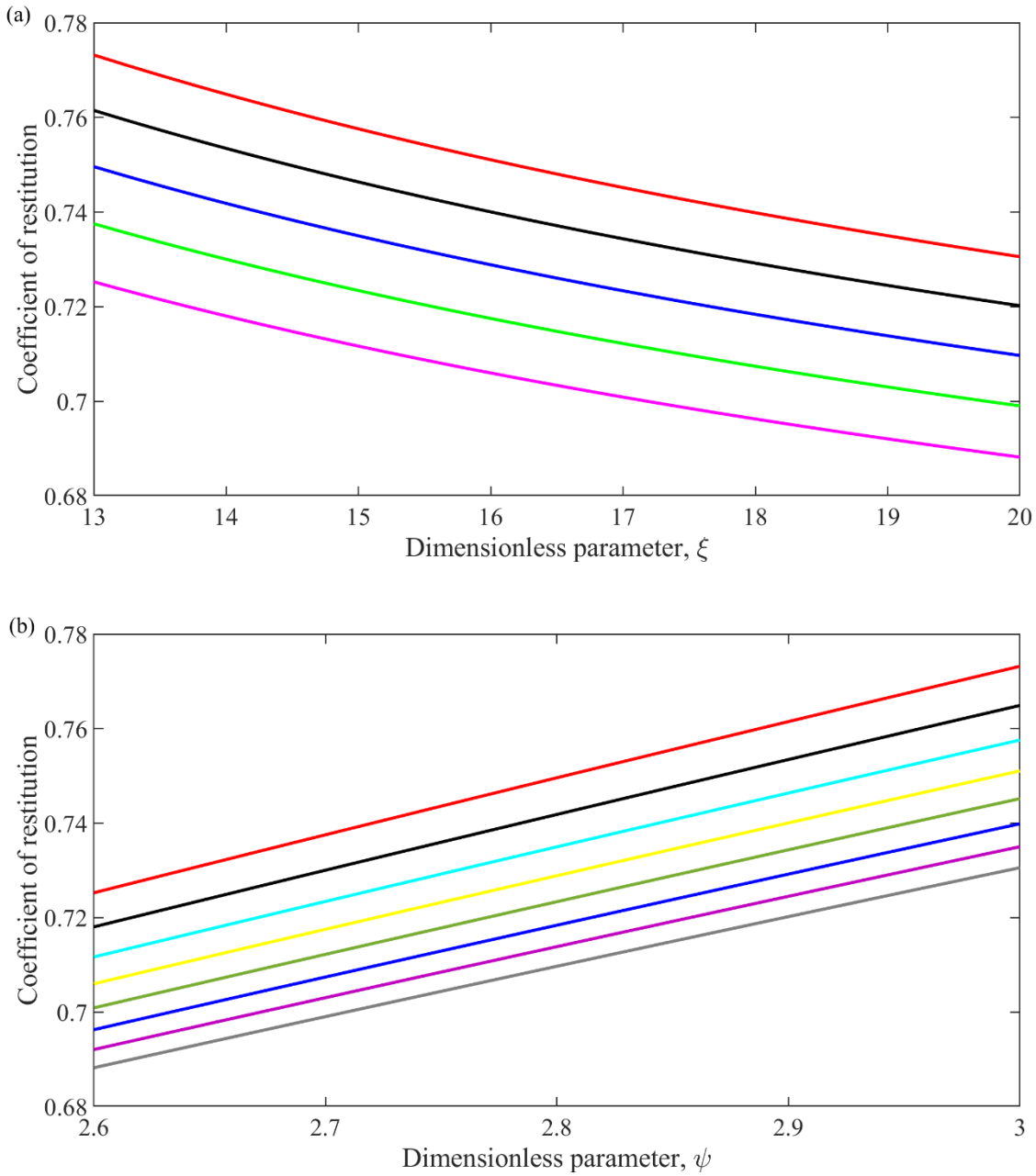

Fig.3 Variations of the CoRs as functions of the dimensionless parameter (a) ξ, where red, black, blue, green, and purple lines correspond to ξ=3.0, 2.9, 2.8, 2.7, and 2.6, respectively; (b) ψ, where red, black, cyan, yellow, green, blue, purple and gray lines correspond to ψ=13, 14, 15, 16, 17, 18, 19 and 20, respectively.

4.1. Comparison analysis in the elastoplastic phase

The dynamic responses of the two colliding spheres shown in Fig. 1 were simulated by using the Ma-Liu model, where their initial impact velocities were set as 4 m/s, and the simulation parameters are listed in Table 1. According to our calculations, the initial kinetic energy of the system was equal to 2.091 J, and the maximum contact deformation was identified at 1.1152E-4 m, which was greater than the critical elastic deformation 1.5788E-6 m. The CoR was calculated as 0.6909 by Eq. (8), and the energy dissipation was equal to 1.0929 J. In fact, the elastoplastic deformation is prone to occur in the collision process, which is related to the material properties of the contact bodies and their initial impact velocities. Thus, for this scenario, the elastoplastic contact phase can be easily activated even

if the initial impact velocity equals to 0.03 m/s. Furthermore, according to the formulation of the critical elastic deformation $\delta_y = \pi^2 R p_y^2 / 4E^2$, when the material of the contact bodies presents large Young's modulus and small yield strength, the elastoplastic deformation may occur under tiny impact velocity. Therefore, when using the existing dynamic dashpot models to calculate the collision behavior under small or moderate initial impact velocities, the elastoplastic deformation cannot be ignored.

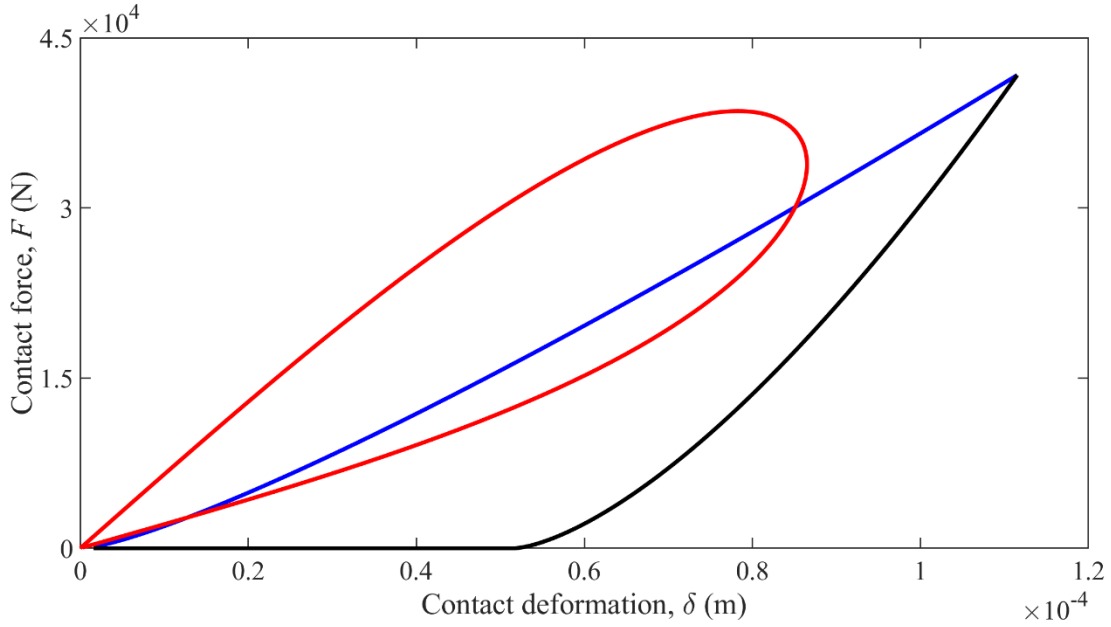

Fig.4 Comparison analysis of the dissipated energies by the new dynamic dashpot model and the Ma-Liu model in the elastoplastic phase, where blue line denotes the elastoplastic deformation in the compression phase, black line denotes the elastoplastic deformation in the recovery phase, and red line represents the new dynamic dashpot model.

Fig. 4 compares the energies dissipated by the new dynamic dashpot model and the Ma-Liu model. The CoR (0.6909) identified using the Ma-Liu model serves as the input parameter to the dynamic dashpot models, including the HC, the LN, the Flores et al., and the new dashpot models. For the new dashpot model, the hysteresis loop (red line) in Fig. 4 depends on integrating the damping term rather than the difference between the loading (blue line) and the unloading paths (black line). When the elastoplastic contact stiffness replaces the Hertz contact stiffness, the energy dissipation obtained from the new dashpot model is the same as the Ma-Liu model, so it is independent of the integration path of the damping term. The work done by the elastoplastic deformation is the main factor that leads energy dissipation during the contact. In other words, the energy dissipation arises from changing the constitutive relation in the compression phase rather than the damping term from the dashpot models. Also, the artificial damping term in the dynamic dashpot model represents the energy dissipation caused by the elastoplastic deformation. Therefore, the post-impact velocities in Table 3 and the maximum contact forces in Table 4 obtained by using the new dashpot model are in agreement with the results obtain from the Ma-Liu model in Fig.5, when the energy dissipation between them during impact can keep consistent with each other. The post-impact velocity shown in Fig. 5 (b) obtained by using the new dashpot model is closed to the result obtained by the Ma-Liu model, since they dissipate similar energy during the contact. Although the error of the maximum contact forces between the Ma-Liu and the new models primarily arises from the redundant damping term in the new model, the new dashpot model is closer to the Ma-Liu model compared to the existing dashpot model.

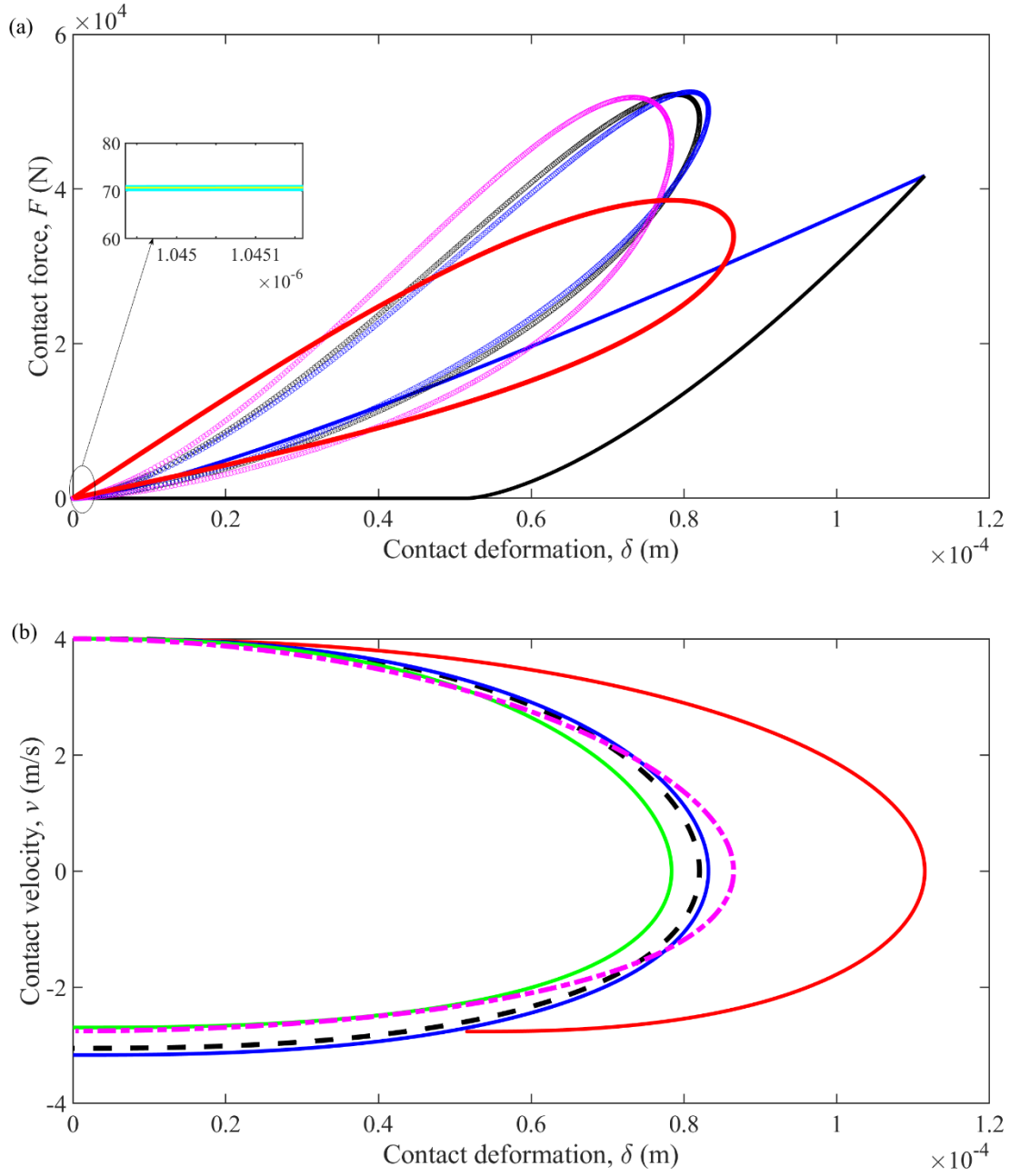

Fig.5 (a) Contact forces of the dynamic dashpot models and the Ma-Liu model in the elastoplastic phase, where cyan line is the elastic deformation in the compression phase, blue line is the elastoplastic deformation in the compression phase, yellow line is the elastic deformation in the recovery phase, black line is the elastoplastic deformation in the recovery phase, red line represents the new dynamic dashpot model, pink circles represents the Flores et al. model, blue circles represents the LN model, and black circles represents the HC model. (b) Contact velocities of the dynamic dashpot models and the Ma-Liu model in the elastoplastic phase, where red line is from the Ma-Liu model, black dashed line is from the HC model, blue line is from the LN model, green line is from the Flores et al. model, and purple dashed line is from the new dynamic dashpot model.

As can be seen from Fig.5 (a), the existing three dynamic dashpot models have different hysteresis damping factors, which leads to the magnitudes of the energy dissipation being significantly different from each other as presented in Table 2. Accordingly, in Fig. 5(b), the motion statuses after impact, including the post-impact velocities listed in Table 3 and the maximum contact force listed in Table 4, are also discrepant from each other. The energy dissipation obtained from the Flores et al. model is

close to the Ma-Liu model; the smaller error arises from that the Hertz contact stiffness overestimates the contact stiffness in the elastoplastic phase.

However, the energy dissipation calculated using the HC model or LN model is conspicuously different from the Ma-Liu model. The main reasons are as follows. (i) Both the HC and the LN models considered that the initial kinetic energy of the contact body could be transformed into strain energy entirely at the end of the compression phase; (ii) Based on the first assumption, the relative impact velocity at any time is described as a function of the maximum contact deformation for the sake of integrating the damping factor. Both models neglected the energy dissipation in the compression phase. On the contrary, the Flores et al. model assumed that a part of its initial kinetic energy is dissipated at the end of the compression phase. Based on this assumption, the impact velocity is expressed as the elliptic function of contact deformation based on a mass-spring-damper model, which eliminates the error from the inaccurate relationship between the impact velocity and the maximum contact deformation. So, the Flores et al. model is more accurate than the HC and the LN models. Furthermore, the post-CoRs obtained by the HC and the LN models are obviously different from the inputted CoR listed in Table 3. The post-CoR from the Flores et al. model is close to the inputted CoR presented in Table 3. Also, the post-impact velocity has a similar situation. In Table 5, the maximum contact forces obtained by using the existing dashpot models have significant discrepancies with the one obtained by the Ma-Liu model. This result reveals that the existing dynamic dashpot models cannot accurately calculate the maximum contact force, which may mislead the design of the mechanical system.

Table 2. Comparison analysis of the energy dissipation evaluated by different contact models

Model	Energy dissipation (J)	Energy dissipation from Ma-Liu model (J)	Error percentage
Hunt-Crossley	0.8727	1.0929	20.15%
Lankarani-Nikravesh	0.7780		28.81%
Flores et al.	1.1356		3.91%
New dashpot model	1.0956		0.25%

Table 3. Post-CoRs and post-impact velocities calculated from different contact models

Model	Velocity (m/s)	Velocity from Ma-Liu model (m/s)	Post-CoR	CoR from Ma-Liu model
Hunt-Crossley	3.0503	2.7636	0.7626	0.6909
Lankarani-Nikravesh	3.1677		0.7919	
Flores et al.	2.6944		0.6736	
New dashpot model	2.7518		0.6880	

Table 4. Maximum Contact forces obtained by different contact models

Model	Contact force (N)	Contact force from Ma-Liu model (N)	Error percentage
Hunt-Crossley	5.2235E4	4.1710E4	25.23%
Lankarani-Nikravesh	5.2544E4		25.97%
Flores et al.	5.1838E4		24.28%
New dashpot model	3.8538E4		7.60%

Therefore, in order to avoid this deficit in the existing dashpot models, it is necessary to develop a new dashpot model by means of the elastoplastic contact stiffness based on the Ma-Liu model. Since the new model in Eq. (18) can maintain the consistency of the energy dissipated during impact with the Ma-Liu model, it can guarantee the accuracies in calculating the post-impact velocity and the maximum contact force. However, it should be noted that this conclusion between the static elastoplastic model and the dynamic dashpot model is inevitable, because they employ completely

different approaches to depicting the elastoplastic collision. Both models have different emphases; in multibody dynamics, the dynamic dashpot model concentrates on the motion status of the contact body after impact, including the maximum contact force and the post-impact velocity; In solid mechanics, the static contact model focuses on the relationship between loading and displacement. They are in a complementary relationship. The new dashpot model improves the existing dashpot models that do not calculate the elastoplastic collision behavior accurately and simplify the calculation process. Therefore, the new dynamic dashpot model provides a new calculation strategy for the elastoplastic collision behavior.

4.2. Comparison analysis in the plastic phase

When the initial impact velocity is set at 8 m/s, the contact will enter the full plastic deformation phase. Likewise, the CoR was identified as 0.6309 by Eq. (8), which was considered as a known parameter for the new dashpot model. As shown in Fig. 6, the energy dissipation (5.0458 J) obtained by using the new model is the same as the one (5.0348 J) obtained by the Ma-Liu model. The error between them is 0.22% as listed in Table 5. In Fig.7, the comparison analysis for the dynamic dashpot models and the Ma-Liu model is also presented.

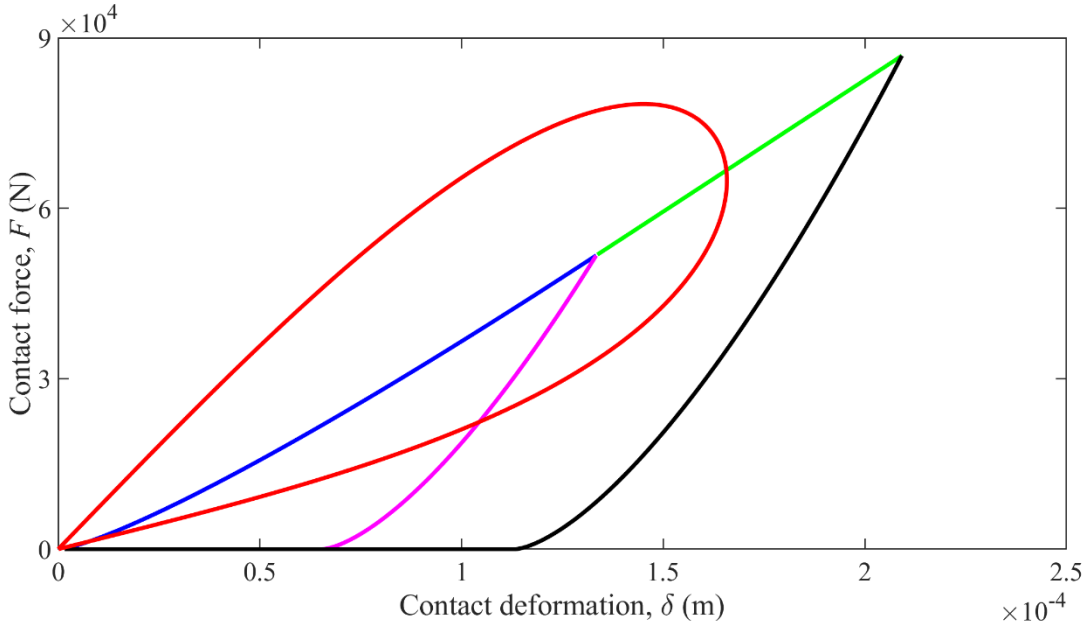

Fig.6 Comparison analysis of the dissipated energies by the new dashpot model and the Ma-Liu model in the plastic phase, where blue line is the elastoplastic deformation in the compression phase, green line is the plastic deformation in the compression phase, purple line is the elastoplastic recovery phase, black line is the plastic deformation in the recovery phase, and red line represents the new dynamic dashpot model.

Table 5. Comparison analysis of the energy dissipation evaluated by different contact models

Model	Energy dissipation (J)	Energy dissipation from Ma-Liu model (J)	Error percentage
Hunt-Crossley	3.9110	5.0348	25.66%
Lankarani-Nikravesh	3.4293		35.22%
Flores et al.	5.2028		3.34%
New dashpot model	5.0458		0.22%

Table 6. Post-CoRs and post-impact velocities calculated from different contact models

Model	Velocity (m/s)	Velocity from Ma-Liu model (m/s)	Post-CoR	CoR from Ma-Liu model

Hunt-Crossley	5.8276	5.0473	0.7285	0.6309
Lankarani-Nikravesh	6.1393		0.7674	
Flores et al.	4.8808		0.6101	
New dashpot model	5.0071		0.6259	

Table 7. Maximum Contact forces obtained by different contact models

Model	Contact force (N)	Contact force from Ma-Liu model (N)	Error percentage
Hunt-Crossley	1.1944E5	8.6858E4	37.51%
Lankarani-Nikravesh	1.2011E5		38.28%
Flores et al.	1.1955E5		37.64%
New dashpot model	7.8359E4		9.78%

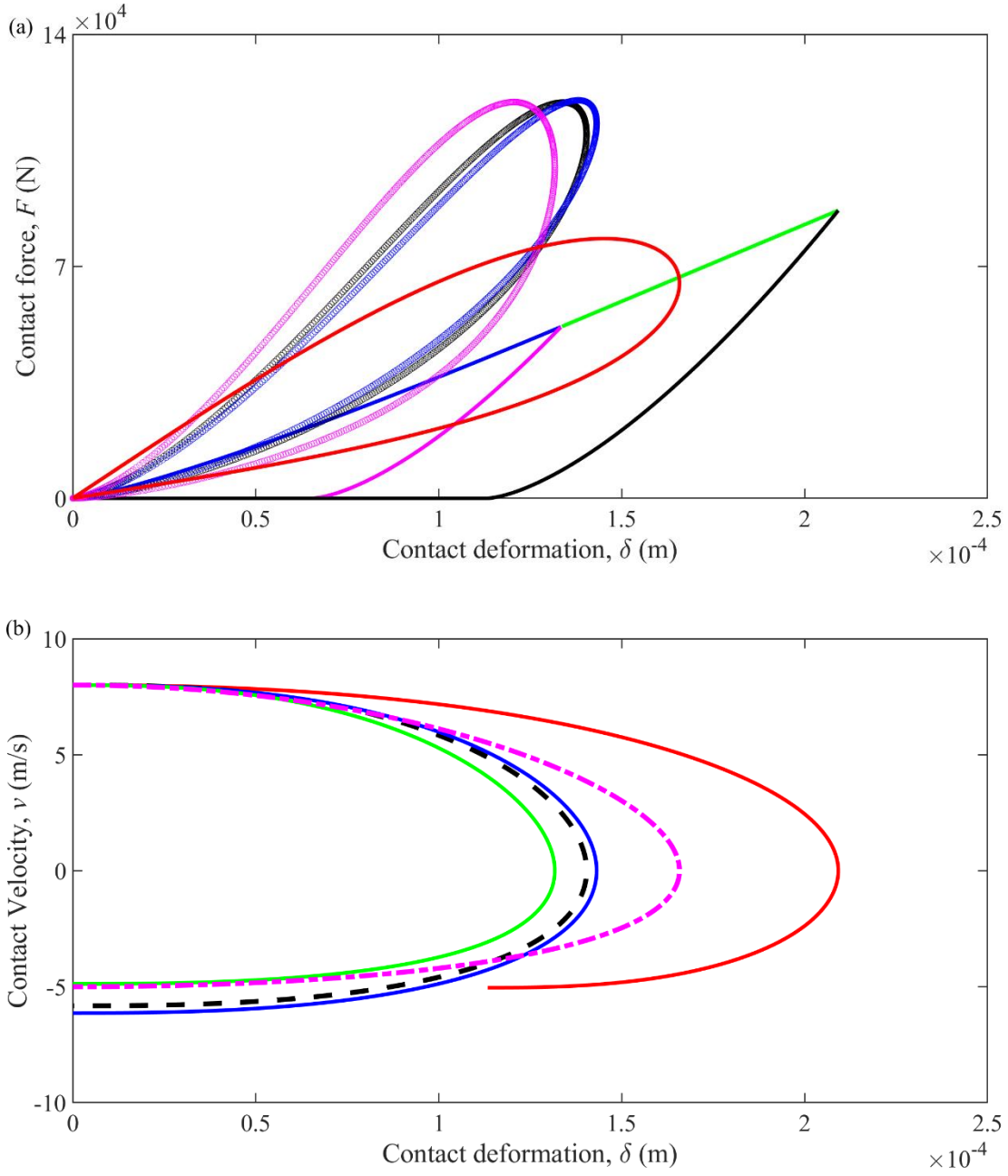

Fig.7 (a) Contact forces of the dynamic dashpot models and the Ma-Liu model in the plastic phase, where blue line is the elastoplastic deformation in the compression phase, green line is the plastic deformation in the compression phase, purple line is the elastoplastic deformation in the recovery phase, black line is the plastic deformation in the

recovery phase, red line represents the new dynamic dashpot model, pink circles represent the Flores et al. model, blue circles represent the LN model, black circles represent the HC model. (b) Contact velocities of the dynamic dashpot models and the Ma-Liu model in the plastic phase, where red line is from the Ma-Liu model, black dashed line is from the HC model, blue line is from the LN model, green line is from the Flores et al. model, and purple dashed line is from the new dynamic dashpot model.

Obviously, when the full plastic deformation is activated, the errors between the existing dashpot models and the Ma-Liu model, including the dissipated energies listed in Table 5, the post-impact velocities shown in Table 6, the maximum contact forces listed in Table 7, are magnified, especially in the maximum contact force. Nevertheless, the new dynamic dashpot model can keep consistent with the Ma-Liu model as demonstrated in Fig. 7, indicating the effectiveness of the new model. More importantly, the CoR in the new dashpot model is not determined by the empirical value anymore, which can be accurately calculated by the Ma-Liu model or simply through a static indentation experiment. This strategy not only enhances the described accuracy of the whole contact behavior, but also provides a method to estimate the CoR for the dashpot model.

5. Numerical simulation

In order to validate the practicability and the rationality of the new dynamic dashpot model, a slider-crank mechanism with a clearance joint and a granular chain were studied in this section as numerical examples.

5.1. Slider-crank mechanism with a clearance joint

In the slider-crank mechanism with a clearance joint shown in Fig.8, the multiple collision between the journal and the bearing happens in a short period when the crank is driven. It is impossible to use the Ma-Liu model to calculate the contact behavior between the clearance joint elements, since the residual deformation and the maximum deformation in each collision need to be identified during the entire operating cycle. So, only the dynamic dashpot model was applied to the dynamic prediction of this mechanism, and we only detected whether the contact between the clearance joint elements happened or not but did not distinguish the compression or the recovery phases, which significantly simplified the calculation process.

In [60], Flores et al. used the LN model to estimate the contact event in the clearance joint. In general, the LN model can accurately describe the energy dissipation when the CoR is greater than 0.9 [12,20,21]. In order to dissipate more kinetic energy to ensure the motion status after impact, Flores et al. [60] assumed the CoR as 0.46. In this case, it is not possible to use the new dynamic dashpot model, as the linearized elastoplastic contact stiffness needs to be determined by the yield strength, Young's modulus, and the Poisson ratio of the contact body, where the yield strength for the contact body was not considered.

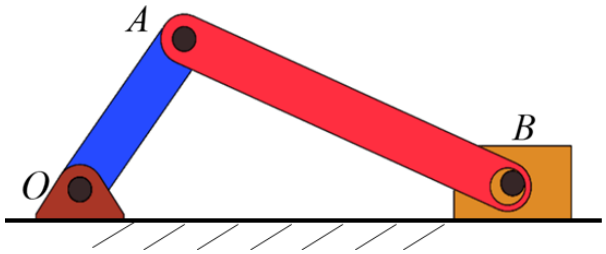

Fig.8 The slider-crank mechanism with a clearance revolute joint. The clearance joint is located at point B between the connecting rod and the slider. The revolute joint is located at point O between the slider and ground, the other revolute joint is located at point A between the slider and connecting rod.

In this study, the dimensionless parameters in the Ma-Liu model were set as $\psi = 3.0$ and $\xi = 13$, according to the material properties of the experiment rig. The yield strengths of the journal and the bearing were 600 Mpa and 20 MPa, respectively. The coefficient of the linear elastoplastic contact stiffness was equal to 6.044E7 N/m. The CoR was identified as 0.54 based on the Ma-Liu model. The critical elastic deformation was equal to 3.7576E-8 m, and the critical plastic deformation was equal to 3.1751E-6 m. The maximum deformation between the journal and the bearing was equal to 1.2923E-5 m under the initial impact velocity at 0.5 m/s, which illuminates the full plastic deformation in the clearance joint is activated in the slider-crank mechanism. The rest of the simulation parameters can be found from [60]. Furthermore, the tangential contact force between the journal and the bearing was estimated based on the modified Coulomb friction model [65]. As can be seen from Fig. 9, simulation result shows that the slider acceleration obtained by using the new dynamic dashpot model is in good agreement with the experimental data in [60]. This comparison demonstrates this accurate calculation approach for the dynamic prediction of the mechanism with clearance joints.

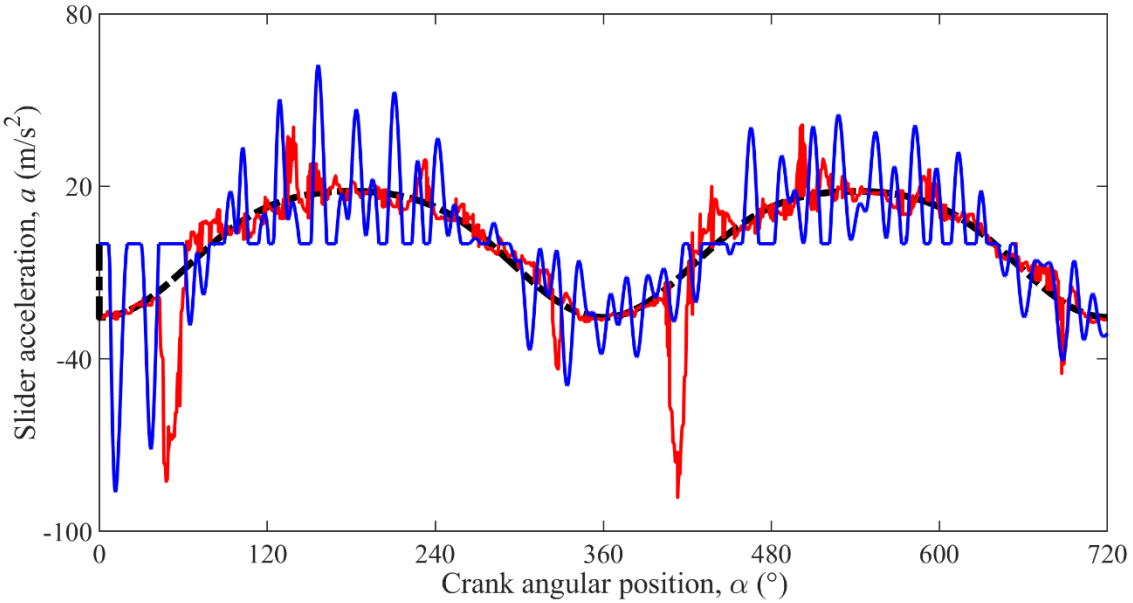

Fig.9 Slider accelerations obtained from the experimental data [60] and the new contact force model, where black dashed line represents the ideal model without the clearance joint, red line denotes the experimental data, and blue line represents the new dynamic dashpot model.

5.2. Horizontal granular chain

Granular chain acts as a shock-absorbing system, which exhibits strongly nonlinear propagations of contact force between particles granules. Most works [66–71] applied the static elastoplastic models to calculate the solitary wave propagation in this system. Fig.10 shows the schematic diagram of the experimental setup developed by Daraio and co-workers [72][59] for a monodisperse granular chain of 70 stainless steel particles assembled horizontally. The particles were made of stainless steel 316, and their size and material properties were identified as listed in Table 8. The striker will impact along the ramp so activating the solitary waves. The contact forces were measured by a calibrated piezo sensor inside the selected particles. The other information about this experimental setup can be found

from [59,72].

The initial impact velocity of the striker was set as 1.77 m/s, and the dimensionless parameters were $\psi = 2.84$ and $\xi = 13$. The critical elastic deformation was equal to 5.4822E-7 m, and the critical plastic deformation was equal to 4.6324E-5 m. According to the contact between the first two spheres, the CoR was identified as 0.81. However, this value cannot be used in the entire granular chain directly, since the actual CoR between two arbitrary granules should be different. Furthermore, the CoR should be less than 0.81 for most of the granular contact behaviors, as more energy should be dissipated via the propagation of the solitary waves. Finally, the CoR was set as 0.65 for the granular chain system.

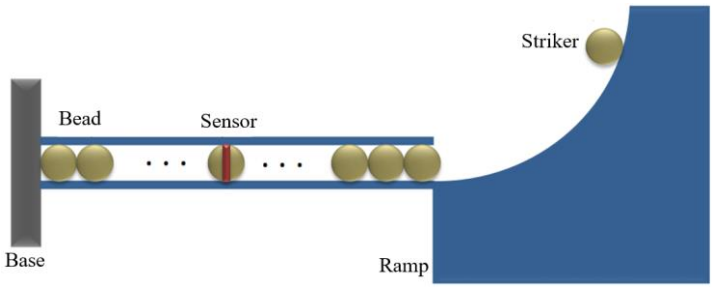

Fig.10 Experimental setup of the one-dimensional granular chain [59]. Solitary waves were activated by a striker granule along the ramp, their contact forces were measured by using calibrated piezo sensors inside the selected beads, and the base was placed on the left-hand side of the rig.

Table 8. Simulation parameters of the granular chain

Parameters	Value
Radius	2.38 mm
Poisson ratio	0.3
Young's modulus	193 GPa
Yield stress	900 MPa
Mass	0.45 g
Position of the sensor (bead number)	9,16,24,31,40,50,56,63

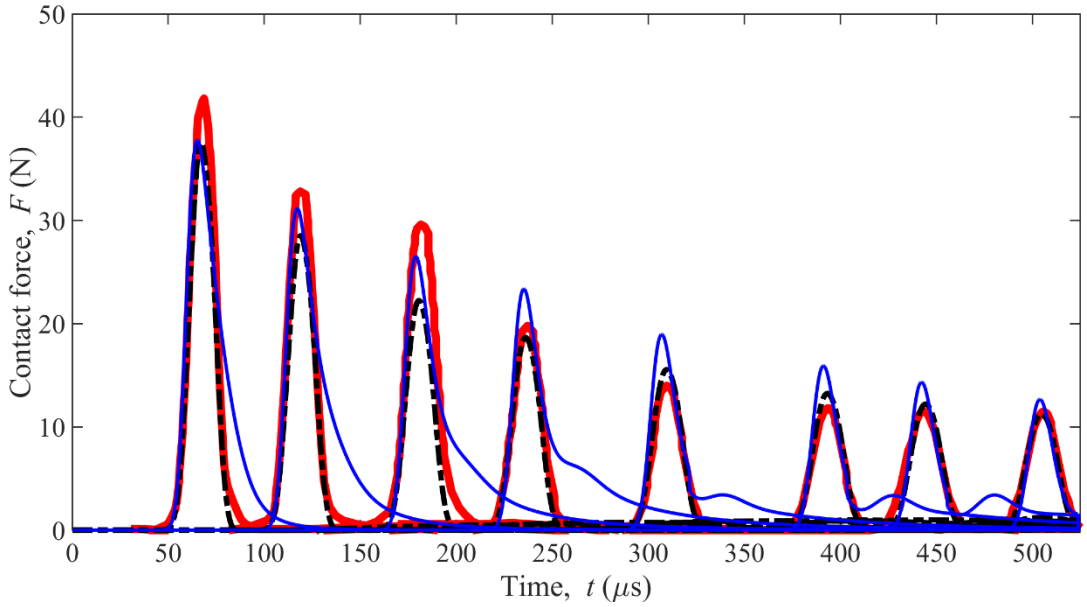

Fig.11 Solitary waves of the granular chain, where red line represents experimental result, black dashed line represents the Ma-Liu model, and blue line represents the new dynamic dashpot model.

According to [73], the peak values of solitary waves of the granular chain reduce with the dissipated energy gradually until the contact behavior reaches the elastic deformation phase. Since the new dynamic dashpot model is mainly applicable to the elastoplastic contact behavior, the contact behavior in the elastoplastic phase is described by the new dashpot model; the contact force in the elastic contact phase will be calculated based on the Flores et al. model. To reproduce the solitary waves in the granular chain based on the new model, the hysteresis damping factor between all granules was assumed as the damping factor between the first two granules with initial impact velocities. This assumption can avoid the numerical singular problem caused by the initial impact velocity of the denominator in damping force, because the granules are stationary in the initial state apart from the striker. In this case, compared to the Ma-Liu model, the new dynamic dashpot model has a redundant term that is the damping term in the elastoplastic or the plastic contact phase. Therefore, the peak values of the solitary wave obtained by using the dashpot model are larger than the ones obtained from the Ma-Liu model as shown in Fig. 11. In addition, the new dynamic dashpot model adopted the same constitutive relation in Eq. (18) to govern the impact behavior in either the compression or the recovery phase. During impact, the dissipated energy was evenly distributed on the hysteresis loop as shown in Fig. 4 and Fig. 6. However, the Ma-Liu model has a different constitutive relation between the compression and the recovery paths; its energy dissipation was described by using the discrepancy between the loading and the unloading paths; namely, the energy was just dissipated at the loading phase. Accordingly, when the contact behavior was in the recovery phase, the contact force obtained from the new model followed the hysteresis loop and became zero when the contact deformation was equal to zero as demonstrated in Fig.4 and Fig.6. Dissimilarly, the contact force estimated by the Ma-Liu model was equal to zero when the contact deformation was equal or smaller than the residual deformation. Thus, the solitary waves shown in Fig.11 calculated by the new model did not fit well with the experimental result at the recovery phase, but coincided with the Ma-Liu model and experimental data at the compression phase. This discrepancy was determined by the constitutive relation of the dashpot model.

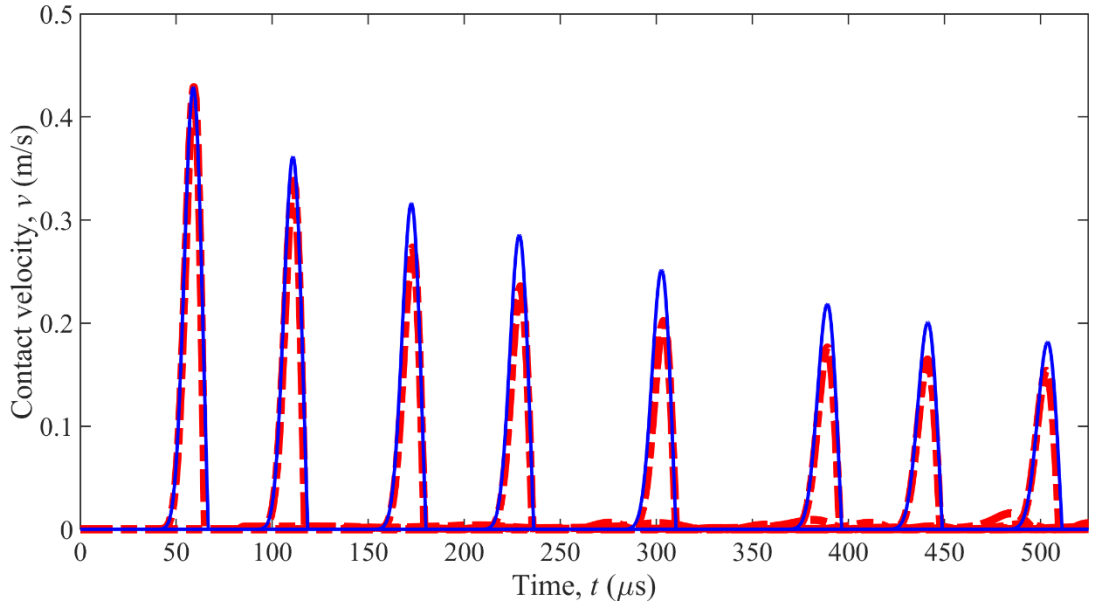

Fig.12 Impact velocities of the new dynamic dashpot model and the Ma-Liu model, where red dashed line represents the Ma-Liu model, and blue line represents the new dynamic dashpot model.

As can be seen from Fig.12, since the dissipated energy described by the new dynamic dashpot

model is almost equivalent to the one dissipated by the Ma-Liu model, their relative contact velocities after impact are also very close. So, the variation tendency of the contact velocities between granules from the new dynamic dashpot model is consistent with the results obtained from the Ma-Liu model. Also, the maximum impact velocities of the solitary waves obtained by the new model are close to the ones obtained by the Ma-Liu model.

The errors between the numerical solution and the experimental data may be introduced by the following reasons: (i) The friction between the particles was not considered in our model assumption; (ii) The effect of the supporting track on the motion status of the particles was neglected; (iii) The sampling error in experimental measurement may also result in discrepancy.

6. Conclusions

In this study, an effective elastoplastic contact model with a new hysteresis damping factor was proposed for the elastoplastic contact behavior in multibody systems. The motivation of this work is that the existing dynamic dashpot models do not accurately describe the energy dissipation during impact, and the available static elastoplastic contact models have limitations due to the sophisticated calculation process.

Firstly, since the Hertz contact stiffness in the existing dynamic dashpot models overestimates the contact stiffness in the elastoplastic or the full plastic phase, it may lose the fidelity in describing energy dissipation during the elastoplastic impact process. This limitation can be eliminated by linearizing the elastoplastic contact stiffness in the Ma-Liu model. On this basis, a new hysteresis damping factor can be derived based on energy conservation and elastoplastic contact stiffness. Subsequently, a new dynamic dashpot model was formulated based on the spring-dashpot model.

Secondly, since the CoR in the new dynamic dashpot model can be accurately identified by the Ma-Liu model, it serves as a bridge to establish the intrinsic connection between the dynamic dashpot model and the static elastoplastic contact models. Our simulation shows that the energy dissipation from the new dynamic dashpot model was almost the same as the Ma-Liu model, ensuring the consistency in evaluating the contact force and the post-impact velocity. This conclusion demonstrates that the energy dissipation during contact is independent of integration path of the damping term in the dynamic dashpot models but depends on the variation of constitutive relation of the contact body. Thus, the impact model can be formulated by the analysis of the static compression.

Finally, compared to the static elastoplastic contact model, the new dynamic dashpot model adopted a new and relatively simplified calculation approach to evaluate the elastoplastic contact behavior in multibody systems. For the slider-crank mechanism with a clearance joint, the slider acceleration obtained by using the new dashpot model was in good agreement with the experimental data. For the granular chain, our simulation shows that the new model can reproduce the propagation of solitary waves and keep consistent with the results obtained from both the Ma-Liu model and the experiment. Therefore, the new dynamic dashpot model is expected to be applied to commercial software, especially for the elastoplastic contact behavior of the grains with initial impact velocity.

Acknowledgements:

This work is supported by the National Natural Science Foundation of China (Grant NO. 11932001, NO.12172004), Fund of the Youth Innovation Team of Shaanxi Universities, and Boya Postdoctoral Fellowship of Peking University.

References

[1] Safaeifar H, Farshidianfar A. A new model of the contact force for the collision between two solid bodies. Multibody Syst Dyn 2020;50:233–57. https://doi.org/10.1007/s11044-020-09732-2.

[2] Lan P, Tian Q, Yu Z. A new absolute nodal coordinate formulation beam element with multilayer circular cross section. Acta Mech Sin Xuebao 2020;36:82–96. https://doi.org/10.1007/s10409-019-00897-4.

[3] Flores P. Contact mechanics for dynamical systems : a comprehensive review. Multibody Syst Dyn 2021. https://doi.org/10.1007/s11044-021-09803-y.

[4] Skrinjar L, Slavič J, Boltežar M. A review of continuous contact-force models in multibody dynamics. Int J Mech Sci 2018;145:171–87. https://doi.org/10.1016/j.ijmecsci.2018.07.010.

[5] Rodrigues da Silva M, Marques F, Tavares da Silva M, Flores P. A compendium of contact force models inspired by Hunt and Crossley's cornerstone work. Mech Mach Theory 2022;167:104501. https://doi.org/10.1016/j.mechmachtheory.2021.104501.

[6] Spitas C, Dwaikat MMS, Spitas V. Non-linear modelling of elastic hysteretic damping in the time domain. Arch Mech 2020;72:323–53. https://doi.org/10.24423/aom.3536.

[7] Osinski Z. Damping of Vibrations. Damping Vib 2018. https://doi.org/10.1201/9781315140742.

[8] Carvalho AS, Martins JM. Exact restitution and generalizations for the Hunt–Crossley contact model. Mech Mach Theory 2019;139:174–94. https://doi.org/10.1016/j.mechmachtheory.2019.03.028.

[9] Glielmo A, Gunkelmann N, Pöschel T. Coefficient of restitution of aspherical particles. Phys Rev E - Stat Nonlinear, Soft Matter Phys 2014;90. https://doi.org/10.1103/PhysRevE.90.052204.

[10] Ahmad M, Ismail KA, Mat F. Impact models and coefficient of restitution: A review. ARPN J Eng Appl Sci 2016;11:6549–55.

[11] Stronge WJ, Sofi AR, Ravani B. Computing the composite coefficient of restitution for inelastic impact of dissimilar bodies. Int J Impact Eng 2019;133:103333. https://doi.org/10.1016/j.ijimpeng.2019.103333.

[12] MacHado M, Moreira P, Flores P, Lankarani HM. Compliant contact force models in multibody dynamics: Evolution of the Hertz contact theory. Mech Mach Theory 2012;53:99–121. https://doi.org/10.1016/j.mechmachtheory.2012.02.010.

[13] Alves J, Peixinho N, Da Silva MT, Flores P, Lankarani HM. A comparative study of the viscoelastic constitutive models for frictionless contact interfaces in solids. Mech Mach Theory 2015;85:172–88. https://doi.org/10.1016/j.mechmachtheory.2014.11.020.

[14] Wang G, Liu C. Further investigation on improved viscoelastic contact force model extended based on hertz's law in multibody system. Mech Mach Theory 2020;153:103986. https://doi.org/10.1016/j.mechmachtheory.2020.103986.

[15] Corral E, Moreno RG, García MJG, Castejón C. Nonlinear phenomena of contact in

multibody systems dynamics: a review. Nonlinear Dyn 2021;104:1269–95. https://doi.org/10.1007/s11071-021-06344-z.
[16] Hunt K, Crossley E. Coefficient of restitution interpreted as damping in vibroimpact. J Appl Mech 1975;42:440–5.
[17] Pereira CM, Ramalho AL, Ambrósio JA. A critical overview of internal and external cylinder contact force models. Nonlinear Dyn 2011;63:681–97. https://doi.org/10.1007/s11071-010-9830-3.
[18] Peng Q, Jin Y, Liu X, Wei YG. Effect of plasticity on the coefficient of restitution of an elastoplastic sphere impacting an elastic plate. Int J Solids Struct 2021;222–223:111036. https://doi.org/10.1016/j.ijsolstr.2021.03.023.
[19] Lee TW, Wang AC. On the dynamics of intermittent-motion mechanisms. Part 1: dynamic model and response. J Mech Transm Autom Des 1983;105:534–40.
[20] Lankarani HM, Nikravesh PE. Continuous contact force models for impact analysis in multibody systems. Nonlinear Dyn 1994;5:193–207. https://doi.org/10.1007/BF00045676.
[21] Lankarani HM, Nikravesh PE. A contact force model with hysteresis damping for impact analysis of multibody systems. J Mech Des Trans ASME 1990;112:369–76. https://doi.org/10.1115/1.2912617.
[22] Adams GG. Imperfectly constrained planer impacts-A coefficient of restitution model. Int J Impact Eng 1997;19:693–701. https://doi.org/10.1016/s0734-743x(96)00053-x.
[23] Hashemnia K. Experimental study of the effect of temperature on the coefficient of restitution of steel balls impact to some industrial metal sheets at elevated temperatures. Powder Technol 2020;368:170–7. https://doi.org/10.1016/j.powtec.2020.04.053.
[24] Zhang Y, Sharf I. Validation of nonlinear viscoelastic contact force models for low speed impact. J Appl Mech Trans ASME 2009;76:1–12. https://doi.org/10.1115/1.3112739.
[25] Thornton C. Coefficient of Restitution for Collinear Collisions of Elastic- Perfectly Plastic Spheres. J Appl Mech 1997;64:383–6.
[26] Ye K, Li L, Hongping Zhu. A note on the Hertz contact model with nonlinear damping for pounding simulation. Earthq Eng Struct Dyn 2009;38:1135–42. https://doi.org/10.1002/eqe.
[27] Flores P, MacHado M, Silva MT, Martins JM. On the continuous contact force models for soft materials in multibody dynamics. Multibody Syst Dyn 2011;25:357–75. https://doi.org/10.1007/s11044-010-9237-4.
[28] Hu G, Hu Z, Jian B, Liu L, Wan H. On the determination of the damping coefficient of non-linear spring-dashpot system to model hertz contact for simulation by discrete element method. J Comput 2011;6:984–8. https://doi.org/10.4304/jcp.6.5.984-988.
[29] Poursina M, Nikravesh PE. Optimal damping coefficient for a class of continuous contact models. Multibody Syst Dyn 2020;50:169–88. https://doi.org/10.1007/s11044-020-09745-x.
[30] Gharib M, Hurmuzlu Y. A New Contact Force Model for Low Coefficient of Restitution Impact. J Appl Meclianics 2012;79:1–6. https://doi.org/10.1115/1.4006494.
[31] Banerjee A, Chanda A, Das R. Historical Origin and Recent Development on Normal Directional Impact Models for Rigid Body Contact Simulation: A Critical Review. Arch Comput Methods Eng 2017;24:397–422. https://doi.org/10.1007/s11831-016-9164-5.
[32] Ma D, Liu C. Contact Law and Coefficient of Restitution in Elastoplastic Spheres. J Appl Mech 2015;82:1–9. https://doi.org/10.1115/1.4031483.
[33] Kim S. Coefficient of restitution for viscoelastic materials. J Korean Phys Soc 2014;64:532–6. https://doi.org/10.3938/jkps.64.532.

[34] Crüger B, Salikov V, Heinrich S, Antonyuk S, Sutkar VS, Deen NG, et al. Coefficient of restitution for particles impacting on wet surfaces: An improved experimental approach. Particuology 2016;25:1–9. https://doi.org/10.1016/j.partic.2015.04.002.
[35] Jackson RL, Green I, Marghitu DB. Predicting the coefficient of restitution of impacting elastic-perfectly plastic spheres. Nonlinear Dyn 2010;60:217–29. https://doi.org/10.1007/s11071-009-9591-z.
[36] Stronge WJ. Contact Problems for Elasto-Plastic Impact in Multi-Body Systems. Impacts Mech. Syst., 2000, p. 189–234. https://doi.org/10.1007/3-540-45501-9_4.
[37] Ghaednia H, Pope SA, Jackson RL, Marghitu DB. A comprehensive study of the elasto-plastic contact of a sphere and a flat. Tribol Int 2016;93:78–90. https://doi.org/10.1016/j.triboint.2015.09.005.
[38] Peng Q, Ye X, Wu H, Liu X, Wei YG. Effect of plasticity on dynamic impact in a journal-bearing system: A planar case. Mech Mach Theory 2020;154. https://doi.org/10.1016/j.mechmachtheory.2020.104034.
[39] Jiang ZH, Liang ZJ, Zhou DW, Deng YJ. Dissipative properties for a ball bouncing on a vertically vibrating plate. Phys A Stat Mech Its Appl 2020;548:123875. https://doi.org/10.1016/j.physa.2019.123875.
[40] Stronge WJ, Sofi AR, Ravani B. Computing the composite coefficient of restitution for inelastic impact of dissimilar bodies. Int J Impact Eng 2019;133:1–11. https://doi.org/10.1016/j.ijimpeng.2019.103333.
[41] Olsson E, Larsson PL. A unified model for the contact behaviour between equal and dissimilar elastic-plastic spherical bodies. Int J Solids Struct 2016;81:23–32. https://doi.org/10.1016/j.ijsolstr.2015.10.004.
[42] Greenwood JA, Williamson JBP. Contact of nominally flat surfaces. Proc R Soc London Ser A Math Phys Sci 1966;295:300–19. https://doi.org/10.1098/rspa.1966.0242.
[43] Zhao Y, Marietta DM, Chang L. An Asperity Microcontact Model Incorporating the Transition From Elastic Deformation to Fully Plastic Flow. J Tribol 2000;122:479–80. https://doi.org/10.1115/1.555389.
[44] Du Y, Wang S. Energy dissipation in normal elastoplastic impact between two spheres. J Appl Mech 2009;76:1–8. https://doi.org/10.1115/1.3130801.
[45] Brake MR. An analytical elastic-perfectly plastic contact model. Int J Solids Struct 2012;49:3129–41. https://doi.org/10.1016/j.ijsolstr.2012.06.013.
[46] Burgoyne HA, Daraio C. Strain-rate-dependent model for the dynamic compression of elastoplastic spheres. Phys Rev E - Stat Nonlinear, Soft Matter Phys 2014;89:1–5. https://doi.org/10.1103/PhysRevE.89.032203.
[47] Bartier O, Hernot X, Mauvoisin G. Theoretical and experimental analysis of contact radius for spherical indentation. Mech Mater 2010;42:640–56. https://doi.org/10.1016/j.mechmat.2010.03.003.
[48] Sandeep CS, Luo L, Senetakis K. Effect of grain size and surface roughness on the normal coefficient of restitution of single grains. Materials (Basel) 2020;13:1–14. https://doi.org/10.3390/ma13040814.
[49] Mei X, Hu X, Zhou Z, Luo G, Wu J. An improved calculation model for predicting the coefficient of restitution and maximum impact force of rockfalls. Arab J Geosci 2020;13:1–10. https://doi.org/10.1007/s12517-020-06020-3.
[50] Li Y, Yang Y, Li M, Liu Y, Huang Y. Dynamics analysis and wear prediction of rigid-flexible

coupling deployable solar array system with clearance joints considering solid lubrication. Mech Syst Signal Process 2022;162:108059. https://doi.org/10.1016/j.ymssp.2021.108059.
[51] Wang H, Zhou C, Wang H, Hu B, Liu Z. A novel contact model for rough surfaces using piecewise linear interpolation and its application in gear wear. Wear 2021;476:203685. https://doi.org/10.1016/j.wear.2021.203685.
[52] Marques F, Roupa I, Silva MT, Flores P, Lankarani HM. Examination and comparison of different methods to model closed loop kinematic chains using Lagrangian formulation with cut joint, clearance joint constraint and elastic joint approaches. Mech Mach Theory 2021;160:104294. https://doi.org/10.1016/j.mechmachtheory.2021.104294.
[53] Dwaikat M. M. S., Spitas C, Spitas V. A non-linear model for elastic hysteresis in the time domain: Implementation for multiple degrees of freedom. Proc Inst Mech Eng Part C J Mech Eng Sci 2021;235:4612–24.
[54] Zhang J, Li W, Zhao L, He G. A continuous contact force model for impact analysis in multibody dynamics. Mech Mach Theory 2020;153:103946. https://doi.org/10.1016/j.mechmachtheory.2020.103946.
[55] Alluhydan K, Razzaghi P, Hurmuzlu Y. On Planar Impacts of Cylinders and Balls. J Appl Mech Trans ASME 2019;86. https://doi.org/10.1115/1.4043143.
[56] Mohajeri MJ, Helmons RLJ, van Rhee C, Schott DL. A hybrid particle-geometric scaling approach for elasto-plastic adhesive DEM contact models. Powder Technol 2020;369:72–87. https://doi.org/10.1016/j.powtec.2020.05.012.
[57] Daraio C, Nesterenko VF, Herbold EB, Jin S. Tunability of solitary wave properties in one-dimensional strongly nonlinear phononic crystals. Phys Rev E - Stat Nonlinear, Soft Matter Phys 2006;73:1–10. https://doi.org/10.1103/PhysRevE.73.026610.
[58] Burgoyne HA, Daraio C. Elastic-plastic wave propagation in uniform and periodic granular chains. J Appl Mech Trans ASME 2015;82:1–10. https://doi.org/10.1115/1.4030458.
[59] Feng Y, Kang W, Ma D, Liu C. Multiple Impacts and Multiple-Compression Process in the Dynamics of Granular Chains. J Comput Nonlinear Dyn 2019;14. https://doi.org/10.1115/1.4044584.
[60] Flores P, Koshy CS, Lankarani HM, Ambrósio J, Claro JCP. Numerical and experimental investigation on multibody systems with revolute clearance joints. Nonlinear Dyn 2011;65:383–98. https://doi.org/10.1007/s11071-010-9899-8.
[61] Rebouças GF d. S, Santos IF, Thomsen JJ. Unilateral vibro-impact systems — Experimental observations against theoretical predictions based on the coefficient of restitution. J Sound Vib 2019;440:346–71. https://doi.org/10.1016/j.jsv.2018.10.037.
[62] Yigit AS, Christoforou AP, Majeed MA. A nonlinear visco-elastoplastic impact model and the coefficient of restitution. Nonlinear Dyn 2011;66:509–21. https://doi.org/10.1007/s11071-010-9929-6.
[63] Weir G, Tallon S. The coefficient of restitution for normal incident, low velocity particle impacts. Chem Eng Sci 2005;60:3637–47. https://doi.org/10.1016/j.ces.2005.01.040.
[64] Rodrigues da Silva M, Marques F, Tavares da Silva M, Flores P. A compendium of contact force models inspired by Hunt and Crossley's cornerstone work. Mech Mach Theory 2022;167:104501. https://doi.org/10.1016/j.mechmachtheory.2021.104501.
[65] Guide AT, Problem LD, Model BY, Your T, Prototype F, Results V, et al. Getting Started Using ADAMS / View n.d.
[66] Hong J, Ji JY, Kim H. Power laws in nonlinear granular chain under gravity. Phys Rev Lett

1999;82:3058–61. https://doi.org/10.1103/PhysRevLett.82.3058.
[67] Hong J. Universal power-law decay of the impulse energy in granular protectors. Phys Rev Lett 2005;94:18–21. https://doi.org/10.1103/PhysRevLett.94.108001.
[68] Job S, Melo F, Sokolow A, Sen S. How hertzian solitary waves interact with boundaries in a 1D granular medium. Phys Rev Lett 2005;94:1–4. https://doi.org/10.1103/PhysRevLett.94.178002.
[69] Nesterenko VF, Daraio C, Herbold EB, Jin S. Anomalous wave reflection at the interface of two strongly nonlinear granular media. Phys Rev Lett 2005;95:1–4. https://doi.org/10.1103/PhysRevLett.95.158702.
[70] Daraio C, Nesterenko VF, Herbold EB, Jin S. Energy trapping and shock disintegration in a composite granular medium. Phys Rev Lett 2006;96:1–4. https://doi.org/10.1103/PhysRevLett.96.058002.
[71] Doney R, Sen S. Decorated, tapered, and highly nonlinear granular chain. Phys Rev Lett 2006;97:1–4. https://doi.org/10.1103/PhysRevLett.97.155502.
[72] Carretero-González R, Khatri D, Porter MA, Kevrekidis PG, Daraio C. Dissipative solitary waves in granular crystals. Phys Rev Lett 2009;102:1–4. https://doi.org/10.1103/PhysRevLett.102.024102.
[73] Pal RK, Awasthi AP, Geubelle PH. Wave propagation in elasto-plastic granular systems. Granul Matter 2013;15:747–58. https://doi.org/10.1007/s10035-013-0449-1.